Long-term Land-Atmosphere Energy and Water Exchange Observational Dataset over central Tibetan Plateau

Haipeng Yu[1], Guantian Wang[2,1,4], Zeyong Hu[1]*, Yaoming Ma[2,3], Maoshan Li[3,4], Weiqiang Ma[2,3], Lianglei Gu[1], Fanglin Sun[1], Hongchun Gao[1], Shujin Wang[1], Fuquan Lu[1,5,4]

[1] Nagqu Plateau Climate and Environment Observation and Research Station of Tibet Autonomous Region, State Key Laboratory of Cryospheric Science and Frozen Soil Engineering, Northwest Institute of Eco-Environment and Resources, Chinese Academy of Sciences, Lanzhou 730000, China

[2] Tianjin Meteorological Observatory, Tianjin 300202, China

[2,3] Land-Atmosphere Interaction and Its Climatic Effects Group, State Key Laboratory of Tibetan Plateau Earth System, Environment and Resources, National Observation and Research Station for Qomolongma Special Atmospheric Processes and Environmental Changes, Institute of Tibetan Plateau Research, Chinese Academy of Sciences, Beijing 100101, China

[3,4] School of Atmospheric Sciences, Plateau Atmosphere and Environment Key Laboratory of Sichuan Province, Chengdu Plain Urban Meteorology and Environment Observation and Research Station of Sichuan Province, Chengdu University of Information Technology, Chengdu 610225, China

[4,5] University of Chinese Academy of Sciences, Beijing 100049, China

Correspondence: Zeyong Hu (zyhu@lzb.ac.cn)

Abstract:In recent decades, the climate of Tibetan Plateau has undergone notable changes, which has a strong influence on global climate systems and human activities, making it a research hotspot. However, due to its extreme elevation, harsh environment, and complex underlying surface, long-term observations of the central Plateau's atmospheric vertical profiles have been challenging and scientific data sharing is crucial and in urgent need. This paper presents a 9-year observational dataset (2014-2022) with hourly temporal resolution from the Nagqu region of northern Tibet. The dataset is a combination of four field stations covering the central Tibetan Plateau, which recorded near-surface meteorological data, radiation budget, turbulent fluxes, and soil hydrothermal characteristics. All observational items in this dataset underwent data processing and quality control to ensure data quality. This dataset represents the most detailed raw observational data on the central Tibetan Plateau's spatial coverage and recent changes. It holds significant value in revealing energy and water exchanges between the land surface and the atmosphere on the Tibetan Plateau. Main datasets are freely available at the National Tibetan Plateau / Third Pole Environment Data Center (https://doi.org/10.11888/Meteoro.tpdc.270010 and https://cstr.cn/18406.11.Meteoro.tpdc.270010, Hu et al., 2019) and additionally at National Tibetan Plateau / Third Pole Environment Data Center (https://doi.org/10.11888/Atmos.tpdc.300325 and https://cstr.cn/18406.11.Atmos.tpdc.300325, Hu et al., 2023).

Key words: field observation, observational dataset, land-atmosphere interaction, Tibetan Plateau, energy and water exchanges

1.Introduction

The Tibetan Plateau (TP), with an average altitude exceeding 4000 meters, is the world's largest mountain range, often referred to as the "Third Pole" (Qiu, 2008). It is the source of many major rivers, including the Yangtze, Yellow, Mekong, and Brahmaputra, which provide freshwater to 1.4 billion people (Immerzeel et al., 2020). It is also known as the "Asian Water Tower" (Immerzeel et al., 2010). The plateau's substantial absorption of solar radiation renders it the warmest region in the mid-troposphere. This plays a key role in the evolution of the East Asian Summer Monsoon and Indian Summer Monsoon systems (Wu et al., 2007; Wu et al., 2012; Li et al., 2018; Zhang et al., 2019), which in turn affect circulation patterns in East Asia, and even the Northern Hemisphere (Fan et al., 2023; Curio and Scherer, 2016; Sun et al., 2022). The intricate surface characteristics of the TP make it particularly susceptible to external disturbances in the context of global warming (Li et al., 2022; Kang et al., 2010). Meteorological observations indicate that surface warming on the TP commenced at an earlier and more accelerated pace than in other regions at the same latitude (Liu and Chen, 2000). Climate change on the TP has resulted in most regions becoming warmer and moister, while the southern part has become warmer and drier (Yang et al., 2014). These changes in temperature and moisture have further led to significant shifts in many environmental systems on the plateau, including precipitation (Yang et al., 2011), glaciers (Yao et al., 2012), lakes (Lei et al., 2014), and vegetation (Shen et al., 2015). Therefore, in-depth research on TP not only helps us better understand the impact of global warming on its unique ecosystems and climatic features, but also is crucial for assessing its contribution to regional and even global water cycles and energy balance. In recent decades, a multitude of comprehensive observation stations have been established with the objective of strengthening climate change research on the TP. These include the Third Pole Environment Observation and Research Platform and the Integrated Three-Dimensional Observation Research Platform for Third Pole Environment (Ma et al., 2018; Ma et al., 2023). The establishment of these observation stations has resulted in a significant improvement in the availability of data on land-atmosphere interactions on the plateau. The comprehensive data network has enhanced the quality of land surface models and corrected satellite retrievals (Ma et al., 2023). However, due to factors such as transportation and maintenance costs, most observations are concentrated in the eastern part of the TP, with limited long-term observations of the plateau's interior, especially in the high-altitude regions of northern Tibet (Shen and Xiong,2016; Duan and Xiao, 2015).

The central Tibetan Plateau (CTP) belongs to a typical plateau climate with an average altitude exceeding 4500 metres. It is bordered by the Kunlun and Tanggula Mountains to the northwest and the Nyenchen Tanglha Mountains to the south, covering an area of 446,000 square kilometres, which represents one-fifth of the total area of Tibet. The CTP is known as the "Roof of the Roof of the World," representing the highest and most typical plateau form on the TP. Due to its high altitude, the substrate is dominated by cold-resistant vegetation, with an annual precipitation of 154.9 mm and approximately 50 rainy days, characterizing a typical subarctic semi-arid monsoon climate (Li et al., 2017). During clear weather, the downward shortwave radiation peaks at 1200 W/m², which is significantly higher than inland observations (He et al., 2010). The period from May to September is characterised by warm and moist conditions, with frequent rainfall, while October to April is cold and dry with prevalent strong winds. During the summer months, the CTP serves as a thermal core area, with surface heating being a key factor in making the plateau a heat source. The thermal effect of the CTP influences not only the plateau itself but also weather and climate systems in East Asia, and even the Northern Hemisphere (Zhao et al.,2019). Over the past 40 years, the warming trend on the CTP has been significantly higher than in lower-altitude areas, with surface temperature warming rates and precipitation amounts also higher than in eastern regions of the TP (Chen et al., 2003; Liu et al., 2009; Yang et al., 2002). The number of

consecutive dry days on the central TP has been steadily decreasing in conjunction with accelerated warming and moistening (Ciwangdunzhu et al., 2018), while its lakes are experiencing strong expansion or contraction (Zhang et al., 2019; Lei et al., 2013 Lei et al., 2014). Some lakes serve as heat sources year-round and have an annual evaporation rate of 312.9mm (Guo et al., 2014). Concurrently, glaciers on the CTP are rapidly melting, and permafrost areas are shrinking, severely impacting the surrounding environment (Jin et al., 2009; Sun et al., 2020). A substantial evidence base indicates that the CTP 's ecological environment is highly fragile, and the surface heat exchange in this region is significant for climate change. However, there remains substantial uncertainty regarding the impact mechanisms (Song et al., 2012; Yang et al., 2014). This can be attributed to the harsh environment, frequent extreme weather such as strong winds and hail showers, and faulty observation equipment. Furthermore, much of the region's intricate topography is unsuitable for human habitation, resulting in a sparsely populated area, inadequate transportation infrastructure, and delayed equipment maintenance. This has led to the availability of relatively limited long-term and stable observational data for the CTP.

To fill these gaps, a series of mesoscale observation networks have been established in the vicinity of the Nagqu Observation Network of Plateau Climate and Environment (NPCE) (Xu et al., 2013). The NPCE commenced observations in 1997 and serves as a link between the East Asian Monsoon and the Indian Monsoon, as well as a transition zone between the monsoon systems and westerly circulation. It is a region of significant thermal activity on the plateau, and the central zone for China's Third Atmospheric Science Experiment on the TP. This distinctive geographical position gives NPCE a pivotal role in TP research. Following decades of observations, data from the Nagqu observing network has become an important platform for research on land-atmosphere interactions in northern Tibet. It has provided significant support for studies on boundary layer observations (Gu et al., 2022; Ueno et al., 2012), land-atmosphere energy transfer (Yang et al., 2010; Gu et al., 2015; Li et al., 2015), substrate evaporation (Zou et al., 2018), soil hydrothermal balance (Bian et al., 2012; Fu et al., 2022), and numerical simulations (Deng et al., 2021; Li et al., 2009; Sun et al., 2020). In recent years, there has been a gradual increase in the availability of field datasets to the public with free access. In order to optimise the potential value of scientific datasets, we describe and provide a high-time-resolution dataset. This dataset comprises nine years of near-surface meteorological, radiation, turbulent flux, and soil hydrothermal observations from NPCE. It provides a more accurate and comprehensive depiction of land-atmosphere interactions and boundary layer structure on the TP, playing a key role in numerical simulations and climate assessments.

The paper is organized as follows: Section 2 provides an overview of NPCE's geographic location, observation equipment, variables, data processing, and data availability. Section 3 presents near-surface meteorological, radiation, turbulent flux, and soil hydrothermal observations, discussing data integrity. Section 4 comprises a discussion, and Section 5 is conclusion.

2. Observation network and data processing

2.1 Site descriptions

The NPCE is affiliated with the Northwest Institute of Eco-Environment and Resources, Chinese Academy of Sciences, was established on 4 May 2009, with observational activities commencing on 1 April 1997. The central station is situated in Niaoqu Village, Luoma Town, Seni District, Nagqu City, Tibet Autonomous Region (longitude 91.90° E, latitude 31.37° N, altitude 4509 metres), near the Tanggula Mountains, where the Indian monsoon and the East Asian monsoon intersect. The observation field is relatively flat and open, with abundant water resources and situated in an area characterised by

pastoral activities. The substrate vegetation is primarily alpine grassland, with a relatively clean atmosphere and a low aerosol content. The station's unique geographic location and subsurface characteristics are significant for the observation and study of high-altitude climate environments.

Over more than 20 years, NPCE has developed into a network of four atmospheric boundary layer physics and land surface process observation points in the Nagqu region and along the Qinghai-Tibet Highway. The locations in Figure 1 are BJ/Nagqu, Amdo, NewD66/Kekexili, and MS3478/Liangdaohe. These represent different substrate characteristics, namely plateau grassland, plateau meadow, plateau wetland, and plateau bareland. Since plant roots are primarily concentrated in the shallow soil layers of the plateau, root biomass in the 0–10 cm layer accounts for 70% of the total root biomass (Su et al., 2021). This leads to pronounced seasonal variations in the surface soil at each observation site. In addition to vegetation, variations in soil temperature and moisture are influenced by precipitation, soil properties, and underlying permafrost. The correlation between soil temperature and air temperature gradually decreases with increasing depth (Wang et al., 2023). Consequently, the different underlying surfaces within the Nagqu observation network represent distinct environmental features of the TP, their interannual variation trends and influencing factors exhibit notable differences (Sun et al., 2015). In 2014, NPCE became a member of the Chinese Academy of Sciences Cold Region Surface Process and Environmental Monitoring Research Network and the Chinese Academy of Sciences Land Surface Process Research Network.
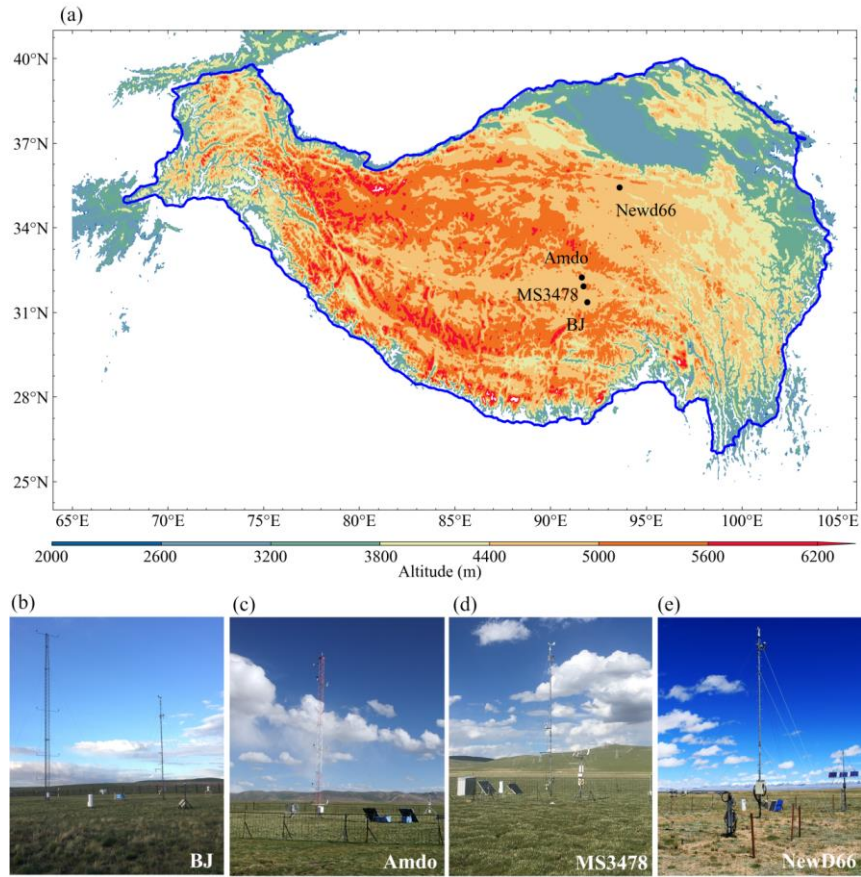
Figure 1. Geographic locations of the observation stations of NPCE (a) and on-site image of BJ (b), Amdo (c), MS3478 (d), and NewD66 (e).

2.2 Observation infrastructure and data processing

The NPCE utilises automatic observation mode, capable of sustaining continuous observation throughout the year. In order to ensure the continuity and accuracy of the observation data, the maintenance engineers are responsible for conducting on-site inspections and maintenance of the infrastructures at regular intervals at each observation station and collect the observation data. All data are transmitted to the data centre for processing to facilitate timely and effective detection of technical problems.

The NPCE near-surface meteorological observation system consists of Planetary Boundary Layer (PBL) towers and Automatic Weather Stations (AWS). These instruments measure vertical profiles of meteorological conditions, including air temperature, relative humidity, wind direction and wind speed within the boundary layer. Observation heights range from 0.75-12 m at BJ and Amdo, and approximately

165 1 m and 10 m at NewD66 and MS3478. The observation probes deployed at each station were of the
166 same type to ensure consistency, but the specific observation heights varied slightly across different
167 stations. The vertical soil hydrothermal characteristics were measured at each station with multilayer soil
168 temperature and moisture probes located between 5-160 cm from the surface, with a proportional
169 distribution of observation depths. High-frequency Eddy Covariance (EC) systems were installed at the
170 four stations after 2012, allowing for the capture of sensible, latent and carbon dioxide fluxes, with a
171 sampling frequency of 0.1 s and an output interval of 30 minutes. Surface observations encompass
172 surface air temperature, humidity, radiative quadrature, atmospheric pressure, precipitation, and snow
173 depth. All observations are recorded at a sampling frequency of 10 seconds and an output interval of 30
174 minutes. More details of the observation instruments are listed in Table 1. Station BJ is also equipped
175 with a ground-based microwave radiometer, a blowing snow observation instrument, and a wind profile
176 radar. The ground-based microwave radiometer (MWP967KV) can observe temperature and humidity
177 profiles up to 10 km above the surface under all weather conditions, with a 2-minute output interval. The
178 FlowCapt FC4 blowing snow sensor inverts digital signals by collecting the acoustic pressure of the
179 blowing snow particles as they impact. The CFL-03 pulsed Doppler wind profile radar (WPR) can
180 capture the wind speed and wind direction profile. It has a detection range of 300 to 3,000 metres and an
181 output interval of 5 minutes. These observational instruments collectively constitute a well-established
182 monitoring system capable of comprehensively tracking weather events across the central TP and their
183 associated impacts.

184 For near-surface micrometeorological observations in complex environments, quality control of
185 data processing is crucial. In order to ensure the consistency of data at each site in the harsh natural
186 environment of the TP, engineers firstly check the data in terms of range, which is a constant value set
187 according to the climatic conditions of the TP and ignore the seasonal variations. Factors such as the
188 replacement of original parts and extreme weather can lead to temporary sensor malfunction. This can
189 result in no change or unrealistic jumps in the data for several hours. These factors can make it difficult
190 to properly deal with the issue during the range check. Consequently, engineers will utilise manual quality
191 control at the conclusion of the process, based on empirical observations, to rectify or eliminate
192 anomalous intervals and thereby ensure that outliers do not adversely affect the mean observations. The
193 removed missing measurements and outliers are denoted by NAN or -9999. Moreover, three categories
194 of quality classification are employed for turbulent fluxes. 0 denotes the highest quality of flux, 1 denotes
195 flux suitable for general analysis, and 2 denotes flux with possible anomalies.

196 Table 1. Detailed information about observation stations and instruments of NPCE.

Site	Variables	Sensor models	Manufacturers	Observation period	Installation height/depth (m)	Units
BJ Lat: 31.37°N Lon: 91.90°E Location:Nagqu Altitude: 4509 m Established in 2001 Plateau Grassland	Air temperature	HMP45D	Vaisala	2001-2018	1.0/2.0/4.0/8.0/16.0/24.0	°C
		HMP155	Vaisala	2012-2022	0.75/1.5/3.0/6.0/12.0/22.0	
	Wind speed and direction	A-5400	Komatsu	2001-2018	10.36	m/s
		WindSonic	Gill	2012- 2022	0.75/1.5/3.0/6.0/12.0/22.0	
	Relative humidity	HMP45D	Vaisala	2001-2018	1.0/2.0/4.0/8.0/16.0/24.0	%
		HMP155	Vaisala	2012-2022	0.75/1.5/3.0/6.0/12.0/22.0	
	Precipitation	NOAH-II	ETI	2001-2018	1.00	mm
		T-200B	Geonor	2012-2022	1.00	
	Soil temperature	TS-301	Okazaki	2001-2018	-0.04/-0.10/-0.20/-0.40	°C
		TR-219	Truwel	2012-2022	-0.05/-0.10/-0.20/-0.40/-0.80/-1.60	
	Soil volumetric water content	Trime EZ	IMKO	2001-2018	-0.04/-0.20	m^{-3}/m^{-3}
		CS616	Campbell	2012-2022	-0.05/-0.10/-0.20/-0.40/-0.80/-1.60	
	Pressure	PTB220C	Vaisala	2001-2022	0.50	hPa
	Downward shortwave radiation	CM21	Kipp&Zonen	2001-2022	1.50	W/m^2
	Upward shortwave radiation	CM21	Kipp&Zonen	2001-2022	1.50	W/m^2
	Downward longwave radiation	PIR	Eppley	2001-2022	1.50	W/m^2
	Soil heat flux	MF-81	EKO	2001-2022	-0.05/-0.10	W/m^2
	Upward longwave radiation	PIR	Eppley	2001-2022	1.50	W/m^2
	Surface sensible heat flux	CSAT3 LI7500A	CAMPBELL CAMPBELL	2008-2022	3.00	W/m^2
	Surface latent heat flux	HMP45AC	VAISALA			

设置了格式: 字体颜色: 自动设置, 上标

Site	Variable	Sensor	Manufacturer	Period	Accuracy/Depth	Units
Amdo Lat: 32.24°N Lon: 91.62°E Location:Amdo Altitude: 4695 m Established in 1997 Plateau Meadow	H$_2$O/CO$_2$ analysis meter	LI7500A	CAMPBELL	2008-2022	3.00	mg/m³
	Air temperature	HMP155	Vaisala	2012-2022	1.5/3.0/6.0/12.0	°C
	Wind speed and direction	WindSonic	Gill	2012-2022	1.5/3.0/6.0/12.0	m/s
	Relative humidity	HMP155	Vaisala	2012-2022	1.5/3.0/6.0/12.0	%
	Precipitation	T-200B	Geonor	2012-2022	1.00	mm
	Soil temperature	TR-219	Truwel	2012-2022	-0.05/-0.10/-0.20/-0.40/-0.80/-1.60	°C
	Soil volumetric water content	CS616	Campbell	2012-2022	-0.05/-0.10/-0.20/-0.40/-0.80/-1.60	m³/m³
	Pressure	PTB220C	Vaisala	2001-2022	0.50	hPa
	Downward shortwave radiation	MS-801	EKO	2012-2022	1.50	W/m²
	Upward shortwave radiation	MS-801	EKO	2012-2022	1.50	W/m²
	Downward longwave radiation	PIR	EPPLEY	2012-2022	1.50	W/m²
	Upward longwave radiation	PIR	EPPLEY	2012-2022	1.50	W/m²
	Soil heat flux	MF-81	EKO	2012-2022	-0.05/-0.10	W/m²
	Surface sensible heat flux / Surface latent heat flux	CSAT3 LI7500A HMP45AC	CAMPBELL CAMPBELL VAISALA	2012-2022	3.00	W/m²
	H$_2$O/CO$_2$ analysis meter	LI7500A	CAMPBELL	2012-2022	3.00	mg/m³
MS3478 Lat: 31.93°N Lon: 91.71°E Location:Liangdaohe Altitude: 4620 m Established in 2001 Plateau Wetland	Air temperature	HMP45D	Vaisala	2001-2022	0.85/9.35	°C
	Wind speed and direction	A-5400	Komatsu	2001-2022	10.35	m/s
	Relative humidity	HMP45D	Vaisala	2001-2022	0.85/9.35	%
	Precipitation	NOAH-II	ETI	2001-2022	1.00	mm
	Soil temperature	TS-301	Okazaki	2001-2022	-0.04/-0.10/-0.20/-0.40	°C
	Soil volumetric water content	Trime EZ	IMKO	2001-2022	-0.04/-0.20	m³/m³
	Pressure	PTB220C	Vaisala	2001-2022	0.5	hPa
	Downward shortwave radiation	CM21	Kipp&Zonen	2001-2022	1.50	W/m²
	Upward shortwave radiation	CM21	Kipp&Zonen	2001-2022	1.50	W/m²
	Downward longwave radiation	PIR	Eppley	2001-2022	1.50	W/m²
	Upward longwave radiation	PIR	Eppley	2001-2022	1.50	W/m²
	Surface sensible heat flux / Surface latent heat flux	CSAT3 LI7500A HMP45AC	CAMPBELL CAMPBELL VAISALA	2012-2022	3.00	W/m²
	H$_2$O/CO$_2$ analysis meter	LI7500A	CAMPBELL	2012-2022	3.00	mg/m³
NewD66 Lat: 35.43°N Lon: 93.59°E Location:Kekexili Altitude: 4465 m Established in 1997 Relocate in 2006 Plateau Bareland	Air temperature	HMP45D	Vaisala	1997-2022	0.60/9.30	°C
	Wind speed and direction	W955-FE	Komatsu	1997-2022	10.40	m/s
	Relative humidity	HMP45D	Vaisala	1997-2022	0.60/9.30	%
	Precipitation	NOAH-II	ETI	1997-2022	1.00	mm
	Soil temperature	TS-301	Okazaki	1997-2022	0.00/-0.01/-0.02/-0.03/-0.04/-0.06/-0.08/-0.10/-0.15/-0.20/-0.40/-0.60/-0.80/-1.00/-1.30/-1.60/-2.00/-2.12	°C
	Soil volumetric water content*	Trime EZ	IMKO	1997-2022	-0.011/-0.04/-0.075/-0.20/-0.40/-0.60/-0.80/-1.00/-1.60/-2.06	m³/m³
	Pressure	PTB210	Vaisala	1997-2022	0.5	hPa
	Downward shortwave radiation	CM21	Kipp&Zonne	1997-2022	1.50	W/m²
	Upward shortwave radiation	CM21	Kipp&Zonne	1997-2022	1.50	W/m²
	Downward longwave radiation	PIR	Eppley	1997-2022	1.50	W/m²
	Upward longwave radiation	PIR	Eppley	1997-2022	1.50	W/m²
	Soil heat flux	MF-81	EKO	1997-2022	-0.05/-0.10	W/m²
	Surface sensible heat flux* / Surface latent heat flux*	CSAT3 LI7500A HMP45AC	CAMPBELL CAMPBELL VAISALA	2012-2022	3.00	W/m²
	H$_2$O/CO$_2$ analysis meter	LI7500A	CAMPBELL	2012-2022	3.00	mg/m³

Note: All data presented herein exhibit availability greater than 50%, with the mark '*' specifically indicating availability below 80%.

3. Data description

3.1 Near-surface meteorological data (Air temperature, relative humidity, wind speed)
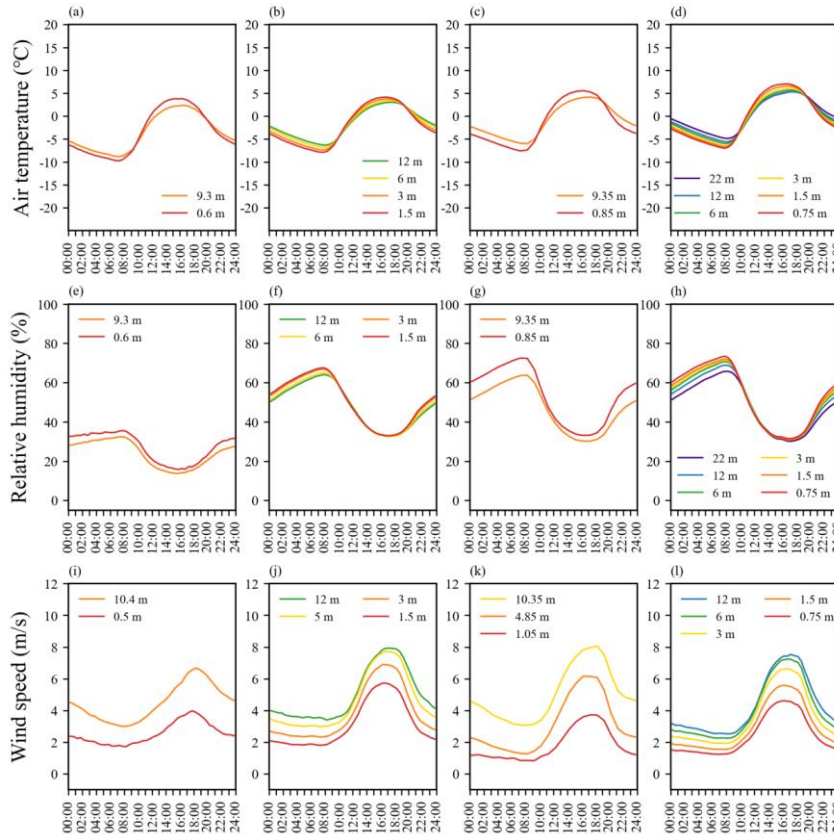
Figure 2. Diurnal variations of temperature at different heights of the PBL tower at NewD66 (a), Amdo (b), MS3478 (c) and BJ (d), with corresponding relative humidity (efgh) and wind speed (ijkl) at each station.

The main variables measured in near-surface micrometeorology are surface temperature, relative humidity and wind speed. Surface air pressure is a single-level observation, which decreases with altitude, while the other variables are gradient observations. Fig. 2 compares the diurnal cycles of temperature, relative humidity and wind speed at different sites to illustrate the micrometeorological characteristics influenced by the different underlying surfaces. Most sites exhibit a maximum temperature at 18:00 and a minimum at 09:00, indicating a clear diurnal pattern. As a result of latitudinal effects, the average temperature at the stations increases from north to south. The northernmost station NewD66 records a minimum temperature of -9.73 ℃ and a maximum of 3.84 ℃, while the southernmost station BJ records a minimum temperature of -7.02 ℃ and a maximum of 7.05 ℃. Irrespective of the water vapour content, relative humidity tends to decrease during the day and increase at night. The most pronounced diurnal variations are observed at lower altitudes. This is because daytime solar radiation heats the surface and atmosphere, making it harder for lower air layers to saturate, which naturally reduces relative humidity. The wind speed generally increases with altitude and shows a diurnal variation, being lower at night and

higher during the day. MS3478 is situated in a plateau wetland, where the abundance of vegetation increases friction with the underlying surface, resulting in significantly reduced surface wind speeds at this station in comparison to other locations.
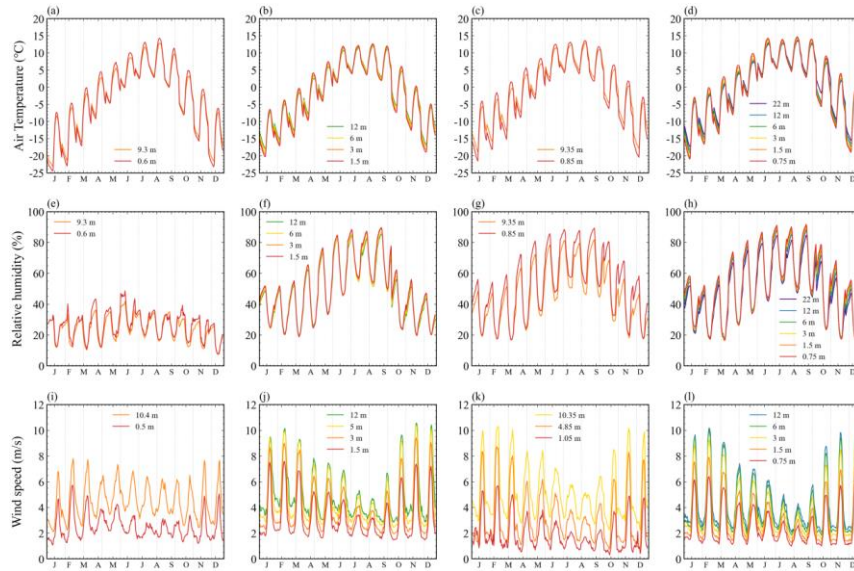
Figure 3. Monthly diurnal variations of temperature at different heights of the PBL tower at NewD66 (a), Amdo (b), MS3478 (c) and BJ (d), with corresponding relative humidity (efgh) and wind speed (ijkl) at each station.

Most stations exhibited notable seasonal fluctuations in temperature, relative humidity and wind speed (Fig. 3). Due to its cold bareland substrate, the NewD66 station experiences more pronounced diurnal temperature variations, with nighttime temperatures lower than those observed at other stations, occasionally reaching below -20 ℃ in January. In summer, with less pronounced diurnal variations than in winter, temperatures peak at all sites, reaching approximately 13 ℃ during the day and approximately 6 ℃ at night. Diurnal variations in relative humidity also show seasonal patterns, with NewD66 remaining consistently lower, never exceeding 50%, and showing small variations in spring and even smaller variations in summer. In contrast, the most pronounced diurnal variations in relative humidity are observed during the spring at the other stations. As water vapour increases over the plateau, nighttime relative humidity remains above 50% at all sites in summer, with diurnal humidity variations gradually decreasing. Wind speeds show greater diurnal variation in winter and increase with altitude. Peak wind speeds of more than 10 m/s are observed at the Amdo and BJ stations. In summer, the 12 m wind speed at the Amdo and BJ sites peaks at 4.31 m/s in August. Surface wind speeds at MS3478 are consistently low, but upper-level wind speeds are similar to those observed at the other sites. Consequently, MS3478 exhibits the most pronounced gradient in wind speed.

243
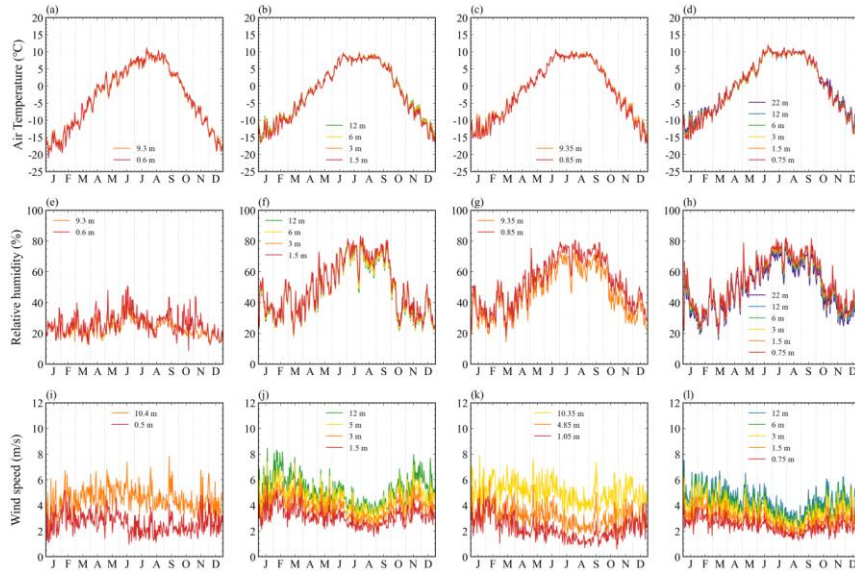
244 Figure 4. Daily mean of temperature at different heights of the PBL tower at NewD66 (a), Amdo (b),

245 MS3478 (c) and BJ (d), with corresponding relative humidity (efgh) and wind speed (ijkl) at each

246 station.

247 Figure 4 presents an annual cycle series, comprising daily mean values derived from gradient

248 observations. At the NewD66 station, winter temperatures are demonstrably lower than at the other

249 stations. In summer, the peak is reached at a later point in time and the duration is shorter. Other stations

250 reach their highest temperatures in June and remain high until early September. With the onset of the

251 monsoon season, continuous water vapour is transported from the ocean to the interior of the TP, resulting

252 in a warming and humidification region. The stations begin to humidify rapidly in early May, reaching a

253 peak in July with daily average relative humidity up to 80%. They then dry rapidly by the end of

254 September, with the end of the monsoon season. The NewD66 station is a plateau bareland, and is only

255 humid for a short period in June, the rest of the year the relative humidity is below 30%. Wind speeds at

256 all stations show a pattern of being lower in summer and higher in winter. The TP is characterised by

257 prevailing westerlies in winter, with daily mean wind speeds reaching 7 m/s. In contrast, the summer

258 months are more humid with frequent changes in weather systems, resulting in average surface wind

259 speeds of less than 4 m/s. Wind speeds at the NewD66 station are lower in winter than at other stations,

260 but higher in summer.

261 Wind directions at the TP differ significantly between the monsoon and non-monsoon seasons (Fig.

262 5). Influenced by the South Asian and East Asian summer monsoons, northeast winds dominate during

263 the monsoon season, accounting for 39% of the observations. In winter, there are fewer weather systems

264 and most of the winds are steady westerly winds, with westerly winds accounting for up to 83% of the

265 observations at different stations. MS3478 records different wind directions than the other stations. It has

266 a consistently high frequency of southeast winds in both summer and winter, probably due to the

267 surrounding topography.
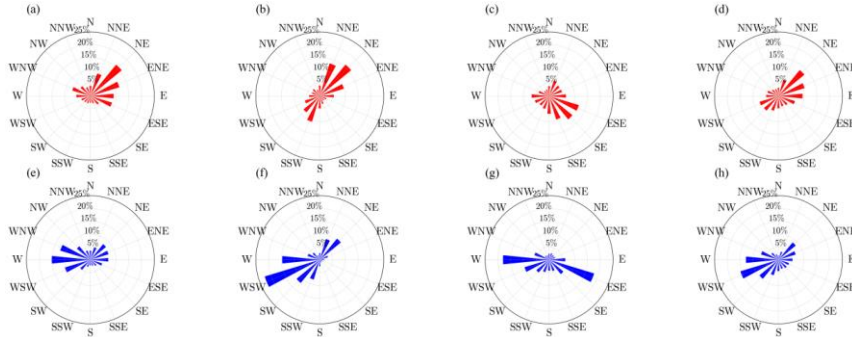
268
269   Figure 5. Wind direction during the monsoon season at NewD66 (a, 10.4 m), Amdo (b, 12.0 m),
270   MS3478 (c, 10.35 m), and BJ (d, 12.0 m), compared to their wind direction during the non-monsoon
271   season (e-h).

3.2 Radiation fluxes

Downward shortwave radiation (Rsd) is the primary source of energy at the surface, and all stations show similar diurnal patterns of Rsd. Observations indicate that the TP begins to absorb solar radiation at 07:00 and stops completely at 21:00 as the sun sets (Fig. 6). The maximum Rsd occurs in the afternoon and reaches 732 W/m². Seasonal variations demonstrate that Rsd is lowest in winter, increases continuously until spring and peaks in May. This is followed by a decrease during the monsoon season, which is likely due to the effects of frequent summer rainfall on the plateau and cloud cover. Since there is little variation in Rsd, differences in upward shortwave radiation (Rsu) are mainly due to variations in surface albedo. The trend in Rsu at all stations is consistent with that of Rsd, with the highest values observed in May, a decrease during the summer months and the minimum in winter. The start and end times of Rsu at each station align with those of Rsd, as illustrated in Figure 5c. MS3478 and BJ stations exhibit slightly lower Rsu values. MS3478 is plateau wetland, and the area near BJ station is a pasture with extensive vegetation cover in summer, which does not strongly reflect sunlight. Consequently, the lower albedo at these two stations results in relatively lower Rsu values. Longwave radiation is influenced by factors such as water vapour content, aerosol content, temperature stratification and cloud thickness. It shows more pronounced seasonal variations than shortwave radiation. The lowest levels of downward longwave radiation (Rld) are observed in winter, while the highest levels are observed in summer. The diurnal variation of Rld is the smallest of the four radiation components, fluctuating within a range of 45 W/m². Upward longwave radiation (Rlu) is minimal in January, increases steadily until June, and stabilises at 370 W/m² during the summer months (June to August). At station MS3478, Rlu is relatively lower, remaining around 350 W/m² during the summer. The minimum of Rlu occurs at 08:00, coinciding with the lowest surface temperatures. The maximum values occur in the afternoon and show greater diurnal variations compared to Rld, with fluctuations up to 140 W/m². Net surface radiation exhibits a clear diurnal cycle, with peaks in the afternoon and slightly negative values at night. This highlights the process of surface heating the atmosphere during the day and cooling it at night. Annual variations show that net surface radiation is highest in summer and lowest in winter.

298
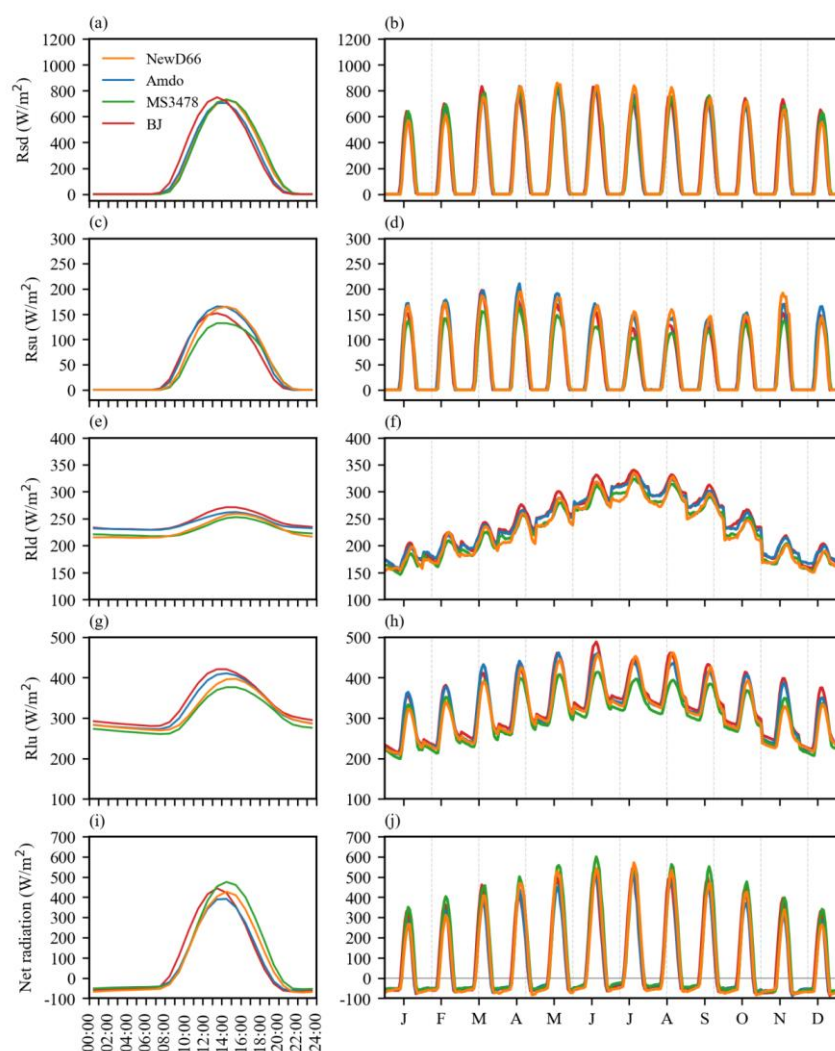
299   Figure 6. Diurnal variations (the first column) and monthly variations of the diurnal (the second

300   column) downward shortwave radiation (a-b), upward shortwave radiation (c-d), downward longwave

301   radiation (e-f), upward longwave radiation (g-h) ,and net radiation (i-j) at the 4 stations.

302

303   **3.3** ~~Sensible heat and latent heat fluxes~~**Surface heat flux and CO$_2$ flux**

設置了格式: 字体颜色: 自动设置, 下标

304   Sensible heat flux (SH) ~~and~~. latent heat flux (LH) and soil hear flux (SHF) are the primary forms

305   of energy transfer between the surface and the atmosphere. Fig. 7 illustrates the monthly diurnal cycles

306   and annual variations of SH and LH at each station. SH is influenced by the temperature difference

307   between the surface and the atmosphere, as well as weather systems associated with precipitation, leading

308   to numerous transient fluctuations. Seasonal variations demonstrate stronger SH at each station in spring

309 and weaker in summer. The daily peaks occur at 14:00, with negative values at night in winter, indicating
310 clear temperature inversions. While net radiation increases steadily in spring, the energy absorbed by the
311 surface before March is mainly used to melt snow. The onset of the monsoon season in May is
312 accompanied by a rapid increase in water vapour on the TP, with a gradual dominance of LH transfer.
313 Consequently, SH peaks in April at each station, with MS3478 (a plateau wetland) peaking in February.
314 The Asian monsoon system transports substantial moisture into the plateau during the summer, resulting
315 in low peaks in sensible heat flux at all stations, with a daily average of 20 W/m². In summer, the NewD66
316 station experiences the highest SH, while the MS3478 station experiences the lowest SH, reflecting the
317 differences in water vapour content between the plateau bareland and plateau wetland.

318

319
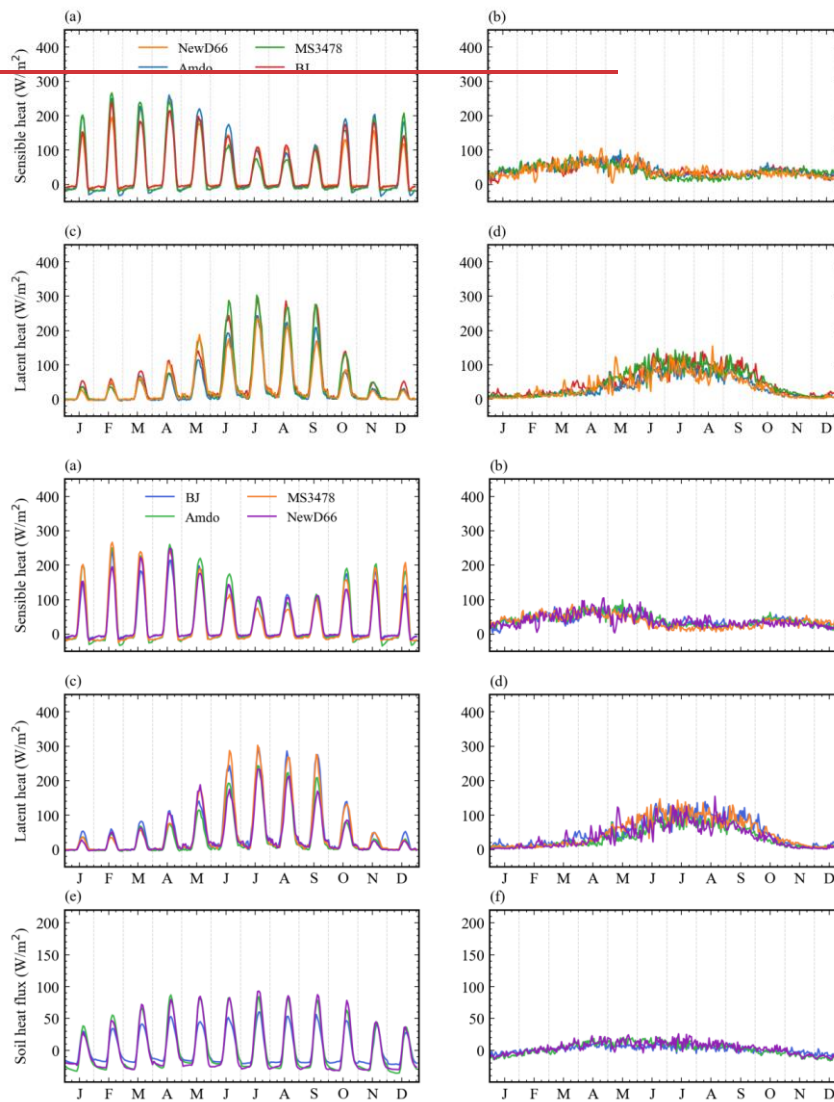
320   Figure 7. Monthly variations of the diurnal (the first column) and daily mean (the second column)

321   sensible heat (a-b), latent heat (c-d), and ~~total~~ soil heat flux (e-f) at the 4 stations.

322

323   The seasonal variation trend of LH is in opposition to that of SH. During the winter, the plateau is
324 characterised by a relatively cold and dry climate, with LH peaks not exceeding 60 W/m² at all stations.
325 As the monsoon season commences in May, LH rapidly rises, maintaining levels above 100 W/m²
326 throughout the summer until it begins to decline in October. Peaks in LH occur in July at all stations,
327 with MS3478's peak appearing earlier in June due to its higher moisture content and remaining high
328 throughout the summer. In winter, nighttime LH approaches zero, but retains weak positive values in
329 summer, indicating that no clear temperature inversions occur at night, and even contributing to heating
330 the atmosphere in the early hours of the night. Fig. 7d shows significant fluctuations in LH during the
331 summer months, which are attributed to the frequent alterations in weather patterns. The diurnal cycle of
332 LH is also influenced by the occurrence of extreme rainfall episodes.

333   SHF is defined as the heat transfer from the land surface to deeper soil layers, is a key component
334 of the surface energy balance. As illustrated in Figure 7ef, the seasonal variation in SHF is relatively
335 moderate compared to SH and LH, with seasonal maxima remaining below 100 W/m². A clear diurnal
336 cycle is observed, characterized by a peak in the afternoon and a minimum during the night. The largest
337 diurnal variation in SHF occurred at Amdo Station from January to April. In contrast, during May to
338 September when surface thermal activity is most intense, Newd66 Station consistently exhibited high
339 levels of diurnal variability. In terms of daily mean values, SHF was highest from May to July and lowest
340 in December. It is noteworthy that Newd66 Station showed the most pronounced diurnal fluctuation,
341 which may be attributed to its plateau bareland underlying surface, which is characterised by a simple
342 composition and high sensitivity to external disturbances. Furthermore, interannual variability was
343 greatest at Newd66 Station, where the amplitude of SHF reached 40 W/m², while at BJ Station, the
344 variation was comparatively subdued, with an amplitude of only 22.7 W/m² throughout the annual cycle.

345
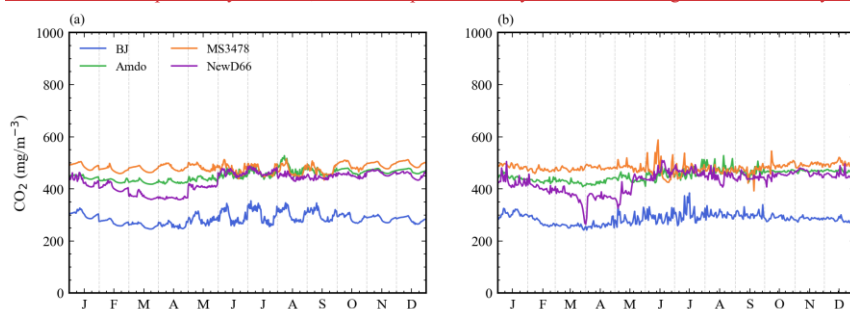
346   Figure 8. Monthly variations of the diurnal (a) and daily mean (b) CO_2 concentration at the 4 stations.

347   As shown in Figure 8a, CO_2 concentrations exhibit a diurnal cycle characterized by an increase
348 during nighttime and a decrease during daytime. This cycle shows minimal monthly variation across the
349 observation period. The NewD66 station displays only a weak diurnal signal between June and August,
350 which may be attributed to the sparse vegetation over the bareland underlying surface, resulting in a
351 relatively limited influence on local CO_2. In contrast, the BJ station, situated near pastureland and remote
352 from human activities, shows relatively lower CO_2 concentrations compared to the other stations, all of
353 which are located within a few kilometres of the Qinghai–Tibet Highway. Figure ~~7~~8b illustrates the
354 annual variation in CO_2 concentration. The BJ station consistently exhibits lower CO_2 levels throughout

设置了格式: 字体颜色: 自动设置, 下标

358 **3.4 Soil hydrothermal characteristics**

359
360 Figure 8 9. Layered soil temperature at NewD66 (a), Amdo (b), MS3478 (c), and BJ (d) observation,
361 and corresponding layered soil moisture (efgh) at each station.

362

363   Soil thermal and moisture variations have a significant impact on energy and moisture exchange
364 between the surface and the atmosphere. Due to varying observation conditions, soil observation depths
365 differ between stations. Fig. 8 9 shows that all stations exhibit a diurnal cycle in soil temperature, with
366 cooling at night and warming during the day. Soil temperature variation diminishes with increasing depth,
367 with 4cm, 10cm, and 20cm depths showing a 2-hour delay in heating and cooling cycles. Significant
368 spatial variation is observed due to differences in soil type, porosity, and substrate. The soil temperature
369 at NewD66 station tends to be lower than at other sites, with 4-cm depths reaching a minimum of -6.56 ℃
370 at night. This is due to a lack of moisture in the surrounding air, which results in a greater daily heating
371 effect, reaching 5.86 ℃ by 16:00. At 160 cm, a slight midday fluctuation is observed, which is not seen
372 at other stations. MS3478, a plateau wetland, exhibits a diurnal variation of 4.29 ℃ at 4-cm depth, with
373 a slight rise at 10 cm at 22:00, and minimal diurnal variation below 10 cm.
374   The diurnal cycle of soil moisture is weak at the shallowest layer, with fluctuations not exceeding
375 0.015 m³/m³. Below 10 cm, soil moisture shows no clear diurnal cycle. The overall soil moisture at
376 NewD66 station is relatively low, but it does not vary linearly with depth. For example, 5-cm depth soil
377 moisture is 0.09 m³/m³, while 160-cm depth moisture remains consistently at 0.17 m³/m³. The soil
378 moisture data from the BJ station exhibits a comparable pattern, with slight fluctuations at the 5-cm depth,
379 maintaining an average of approximately 0.13 m³/m³, and negligible variation at the 160-cm depth,
380 remaining at 0.15 m³/m³. In contrast, the soil moisture at the 160-cm depth from Amdo is considerably
381 lower than that observed in the shallow layers, likely due to the presence of a permafrost layer, which
382 results in a consistently low liquid water content. MS3478's soil moisture exhibits no significant diurnal
383 variation, with 4-cm depth soil moisture averaging 0.22 m³/m³ and 20-cm depth soil moisture averaging
384 0.13 m³/m³, which are both significantly higher than those observed at other stations.
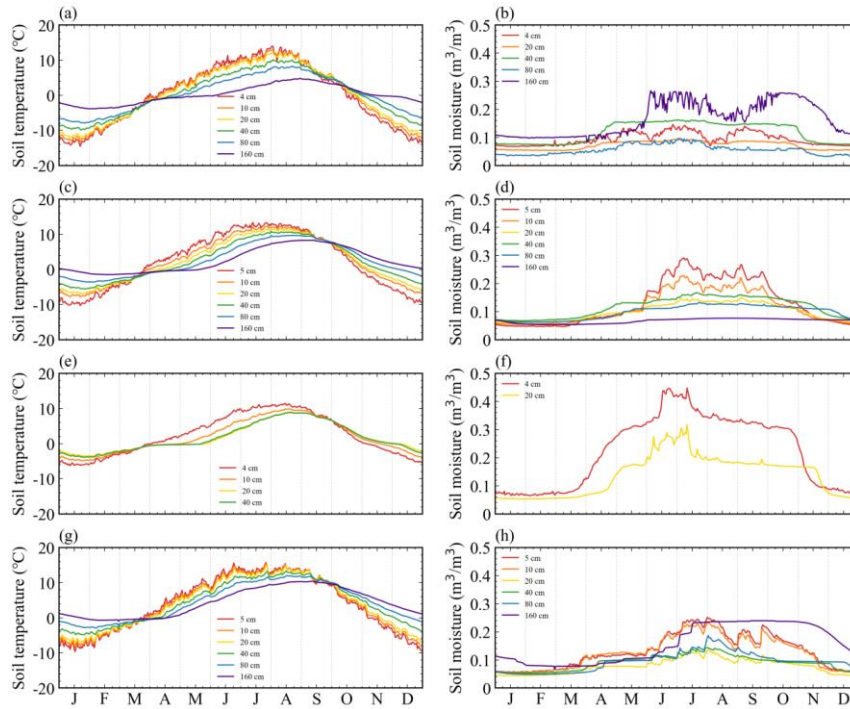
Figure 9̶10. Daily mean soil temperature (a) and soil moisture (b) at NewD66,
same in Amdo (cd), MS3478 (ef), and BJ (gh).

Soil temperature and moisture exhibit clear annual variations at each station, with soil temperature delaying more with increasing observation depth (Fig. 9̶10). Surface soil temperatures peak in July, 40-cm depth temperatures in August, and 160-cm depth temperatures in September. The greatest annual variation in soil temperature is observed in NewD66's 4-cm depth soil temperature, reaching 28.56 ℃, while the smallest is observed in MS3478's, at 17.74 ℃. A similar trend is observed in soil moisture, with higher levels observed in summer and lower levels in winter. Soil moisture increases in spring due to the melting of snow and ice, and in summer due to precipitation. In the absence of rainfall, surface evaporation and runoff results in a rapid decrease in soil moisture. There are significant differences in soil moisture between stations, with substantial fluctuations in surface moisture, indicating vertical variation in the soil moisture profile. NewD66's 4-cm depth soil moisture exhibits minimal annual variation, increasing by only 0.05 m³/m³ in summer. However, 160-cm depth moisture rapidly increases to 0.24 m³/m³ in summer, then gradually decreases in November, coinciding with the point at which 160-cm depth soil temperatures exceed 0 ℃. The soil moisture at all layers of Amdo is below 0.1 m³/m³ in winter, with 5-cm depth moisture reaching 0.29 m³/m³ in summer, and decreasing with increasing depth. MS3478's humid air contributes to higher soil moisture, with 4-cm depth moisture maintaining levels above 0.3 m³/m³ from May to October, even exceeding 0.8 m³/m³ at times. BJ's 4-cm depth moisture rises in April, peaking in August at 0.25 m³/m³. The lowest 20-cm depth moisture is observed year-round, at only 0.12 m³/m³ in July. The 160-cm depth moisture rapidly rises in June, maintaining 0.24 m³/m³ until November.

4. Data availability

Near-surface micrometeorology, soil hydrothermal characteristics, and turbulent flux observation datasets are openly available from the National Cryosphere Desert Data Center and the National Tibetan Plateau Data Center (https://www.ncdc.ac.cn/portal; https://data.tpdc.ac.cn/allData). Following a rigorous screening process that included the identification and elimination of missing values, the physical range check, and the manual quality control, valid data in CSV format is available for download. The file names adhere to the convention of station_datatype_year.csv, and all data files utilise UTC+8 as the designated time standard. Each CSV-formatted data file name includes the name of the variable, the observed height/depth, and the unit.

5. Conclusion and Discussion

As demonstrated in previous sections, the NPCE reliably reflects the characteristics of various variables across different underlying surface and temporal scales, thereby showcasing the reliability and completeness of the data. The challenging environment and dispersed stations on the CTP make it difficult to maintain equipment~~.~~ Frequent extreme weather events contribute to recurrent instrument malfunctions, such as sensor drift, calibration error, environmental interference, and power supply issues. These constraints further highlight the value and importance of the data collected under such demanding conditions. ~~which makes the data collected valuable.~~ The scarcity of field observation data has long been a barrier to in-depth research on the TP. Thus, long-term observations and scientific data sharing are crucial for research on the plateau. This paper introduces land-atmosphere interaction data from several observation stations centred around Nagqu. The dataset comprises 9 years (2014-2022) of hourly continuous series of near-surface meteorological, radiation, turbulent flux, and soil hydrothermal characteristics. This enables effective exploration of the entire process of land-atmosphere interactions on the plateau. Additionally, all data were manually checked for outliers and subjected to quality control. The long-term half-hourly dataset from NPCE provides the opportunity to conduct high-precision numerical simulations at the local level. This enables in-depth research to be conducted on the mechanisms by which the land and atmosphere interact on the plateau and also provides support for comprehensive research into the plateau's energy and water cycles and climate change.

The NPCE is a comprehensive research platform with the primary goal of observing and studying the impacts of weather and climate change on the Tibetan Plateau, water resource utilisation, ecological environmental protection, and human activities. The main objective of the NPCE is based on a plateau climate and the water-energy cycle. In recent years, a range of processes have been the focus of detailed analysis, including non-homogeneous terrain turbulence transfer mechanisms, radiation balance components and energy allocation processes. The analysis has been informed by long-term in situ meteorological observations (Huang et al., 2016). The spatial and temporal variability of SH and LH under complex topographic forcing is a particular highlight (Xie et al., 2018), and energy closure in the central part of the northern Tibetan plateau is further discussed (Li et al., 2015; Li et al., 2016). Satellite-derived products have been utilised to address the spatial representation limitations inherent in field observations (Ma et al., 2014; Ma et al., 2009; Ma et al., 2006). Furthermore, ground-based observations were utilised to validate and calibrate the remote sensing estimates of sensed LH, thereby improving the accuracy of the remote sensing algorithms (Zhong et al., 2019). A distributed sensor network was utilised to monitor soil temperature and humidity gradients, thereby enabling the systematic quantification of the disparities in soil moisture and heat fluxes between permafrost and seasonal permafrost. In these areas,

451 phase change LH associated with freeze-thaw transitions have been demonstrated to influence surface
452 energy distribution (Liu et al., 2015; Fu et al., 2022). A comprehensive analysis of the pattern of
453 boundary layer changes on the CTP has been conducted utilising PBL towers, as well as MWR and
454 radiosonde data (Wang et al., 2025; Sun et al., 2021; Sun et al., 2020). The integration of multi-source
455 observations (Near-surface meteorological data, EC system, boundary layer observation, and satellite
456 inversion) has modified the model representation of land-atmosphere energy balance processes, and
457 further refinement of the parameterisation scheme has been applied to soil freeze-thaw processes (Deng
458 et al., 2021). The enhanced numerical simulation accuracy of blowing snow processes in the CLM model
459 facilitates a more profound comprehension of surface processes and cryosphere changes in local area
460 (Xie et al., 2023; Xie et al., 2021).

461 The data presented in the paper is the average result after filtering out missing values. However, in
462 practical applications, considering the difficulty of instrument maintenance, there may inevitably be
463 anomalies or data discontinuities. As a key observation project on the CTP, the NPCE is implementing
464 an ambitious plan to enhance its monitoring capabilities for understanding global climate dynamics due
465 to its high altitude and ecological sensitivity. This initiative focuses on acquiring advanced
466 instrumentation and expanding monitoring sites to deepen insights into atmospheric, hydrological, and
467 ecological processes, particularly in the CTP and the upper Nu River (Salween River) basin. For
468 instrument acquisition, the station will deploy Raman lidar systems, which are highly specialized for
469 simultaneous detection of water vapor and aerosols in the lower atmosphere. These Raman lidar systems
470 utilize laser-based spectroscopy to provide high-resolution measurements of water vapor concentrations,
471 enabling detailed analysis of moisture transport and its influence on regional climate patterns.
472 Additionally, the same Raman lidar systems will measure aerosol properties, such as particle size,
473 concentration, and distribution, which are essential for studying air quality, aerosol-cloud interactions,
474 and their impact on radiative forcing in the plateau's unique environment. To complement these
475 atmospheric measurements, the station will acquire advanced greenhouse gas analyzers specifically
476 designed to monitor carbon dioxide and methane fluxes from soil and vegetation respiration, providing
477 critical data on biogeochemical cycles and the carbon dynamics of high-altitude ecosystems under
478 changing climatic conditions.

479 The site expansion plan involves establishing new monitoring stations on the CTP and the upper Nu
480 River basin to broaden the scope of environmental observations. The CTP, with its expansive high-
481 altitude grasslands, offers a unique setting to study the interplay between atmospheric processes and
482 ecosystem responses to climate change. Similarly, the upper Nu River basin, a vital hydrological region,
483 will host new sites to investigate water cycles, soil moisture dynamics, and vegetation responses to
484 environmental shifts. By expanding coverage in the upstream Nu River, the station aims to capture spatial
485 and temporal variations in hydrological and ecological parameters, supporting research on water resource
486 management, ecosystem resilience, and climate adaptation strategies in this ecologically sensitive area.

487
488

489 **Acknowledgements**
490 This work was jointly supported by Science and Technology Projects of Xizang Autonomous
491 Region, China (XZ202501JD0022), the National Natural Science Foundation of China (42330609,
492 U2442207), the Youth Innovation Promotion Association of Chinese Academy of Sciences (2021427),
493 the West Light Foundation (xbzg-zdsys-202409) of the Chinese Academy of Sciences, Key talent project
494 in Gansu and Central Guidance Fund for Local Science and Technology Development Projects in Gansu

(No.24ZYQA031). We also acknowledge the Computing Center in Xi'an for providing the computing resources.

Author contributions

All the authors were involved in the generation of the introduced dataset. HY, GW, FS and FL wrote the manuscript with contributions from all the other authors.

References

Bian, L., Gao Z., Ma Y., Koike T., Ma Y., Li Y., Sun J., Hu Z. and Xu X.: Seasonal Variation in Turbulent Fluxes over Tibetan Plateau and Its Surrounding Areas: Research Note, Journal of the Meteorological Society of Japan., 90C, 157-171, 2012.

Ciwangdunzhu, Du J. and Danzengcuojie: Spatial-temporal Change of Consecutive Dry Days in Changtang National Nature Reserve of Tibet During 1971-2017, Chinese Agricultural Science Bulletin, 34(30),118-122, 2018. (in Chinese).

Chen, B., Chao W. and Liu X.: Enhanced climatic warming in the Tibetan plateau due to doubling CO2: A model study, Climate Dynamics, 20(4), 401–413, 2003.

Curio, J. and Scherer D.: Seasonality and spatial variability of dynamic precipitation controls on the Tibetan Plateau, Earth System Dynamics, 7(3), 767-782, 2016.

Deng, M., Meng X., Lu Y., Li Z., Zhao L., Hu Z., Chen H., Shang L., Wang S. and Li Q.: Impact and sensitivity analysis of soil water and heat transfer parameterizations in Community Land Surface Model on the Tibetan Plateau, Journal of Advances in Modeling Earth Systems, 13(9), e2021MS002670, 2021.

Duan, A. and Xiao Z.: Does the climate warming hiatus exist over the Tibetan Plateau? Scientific reports 5(1), 13711, 2015.

Fan, X., Li Y. and Li L.: Synoptic-Scale Effects of Atmospheric Heat Source over Key Areas of the Tibetan Plateau on Its Downstream Rainfall in Summer, Journal of Climate, 36(11), 3647-3666, 2023.

Fu, C., Hu Z., Yang Y., Deng M., Yu H., Lu S., Wu D. and Fan W.: Responses of Soil Freeze-Thaw Processes to Climate on the Tibetan Plateau from 1980 to 2016, Remote Sensing, 14(23), 5907, 2022.

Gu, L., Yao J., Hu Z. and Zhao L.: Comparison of the surface energy budget between regions of seasonally frozen ground and permafrost on the Tibetan Plateau, Atmospheric Research, 153, 553-564, 2015.

Gu, L., Yao J., Hu Z., Ma Y., Sun F., Yu H., Wang S., Yang Y., Guo R. and Qin Y.: Characteristics of the atmospheric boundary layer's structure and heating (cooling) rate in summer over the Northern Tibetan Plateau, Atmospheric Research, 269, 106045, 2022.

Guo, Y., Zhang Y., Ma Y., Ma N.: Surface heat source intensity and surface water/energy balance in Shuanghu, northern Tibetan Plateau, Acta Geographica Sinica, 69(07),983-992, 2014.

He, H., Hu Z., Xun X., Hao L., Gu L., Sun J. and Xu L.: The variation characteristics of surface radiation in wetlands on the northern Tibetan Plateau, Acta Energiae Solaris Sinica, 31(05),561-567, 2010. (in Chinese).

537 Huang, F. and Ma W.: Analysis of Long-Term Meteorological Observation for Weather and Climate
538   Fundamental Data over the Northern Tibetan Plateau, Advances in Meteorology, 2016(1),
539   4878353, 2016.
540 Immerzeel, W., Lutz A., Andrade M., Bahl A., Biemans H., Bolch T., Hyde S., Brumby S., Davies B.,
541   Elmore A., Emmer A., Feng M., Fernández A., Haritashya U., Kargel J., Koppes M.,
542   Kraaijenbrink P., Kulkarni A., Mayewski P., Nepal S., Pacheco P., Painter T., Pellicciotti F.,
543   Rajaram H., Rupper S., Sinisalo A., Shrestha A., Viviroli D., Wada Y., Xiao C., Yao T. and
544   Baillie J.: Importance and vulnerability of the world's water towers, Nature, 577(7790), 364-
545   369, 2020.
546 Immerzeel, Van Beek L. and Bierkens M.: Climate change will affect the Asian water towers, science,
547   328(5984), 1382-1385, 2010.
548 Jin, H., He R., Cheng G., Wu Q., Wang S., Lü L. and Chang X.: Changes in frozen ground in the Source
549   Area of the Yellow River on the Qinghai–Tibet Plateau, China, and their eco-environmental
550   impacts, Environmental Research Letters, 4(4), 045206, 2009.
551 Kang, S., Xu Y., You Q., Flügel W., Pepin N. and Yao T.: Review of climate and cryospheric change in
552   the Tibetan Plateau, Environmental research letters, 5(1), 015101, 2010.
553 Lei, Y., Yang K., Wang B., Sheng Y., Bird B., Zhang G. and Tian L.: Response of inland lake dynamics
554   over the Tibetan Plateau to climate change, Climatic Change, 125, 281-290, 2014.
555 Lei, Y., Yao T., Bird B., Yang K., Zhai J. and Sheng Y.: Coherent lake growth on the central Tibetan
556   Plateau since the 1970s: Characterization and attribution, Journal of Hydrology, 483, 61-67,
557   2013.
558 Li, L., Liu Q., Zhang Y., Liu L., Ding M. and Gu C.: Spatial distribution and variation of precipitation
559   in the Qiangtang Plateau, Geographical Research, 36(11),2047-2060, 2017. (in Chinese)
560 Li, G., Chen H., Xu M., Zhao C., Zhong L., Li R., Fu Y. and Gao Y.: Impacts of topographic complexity
561   on modeling moisture transport and precipitation over the Tibetan Plateau in summer, Advances
562   in Atmospheric Sciences, 39(7), 1151-1166, 2022.
563 Li, M., Babel W., Chen X., Zhang L., Sun F., Wang B., Ma Y., Hu Z. and Foken T.: A 3-year dataset of
564   sensible and latent heat fluxes from the Tibetan Plateau, derived using eddy covariance
565   measurements, Theoretical and Applied Climatology, 122(3-4), 457-469, 2015.
566 Li, M., Su Z., Ma Y., Chen X., Zhang L. and Hu Z.: Characteristics of land-atmosphere energy and
567   turbulent fluxes over the plateau steppe in central Tibetan Plateau, Sciences in cold and arid
568   regions, 8(2), 103-115, 2016.
569 Li, W., Guo W., Qiu B., Xue Y., Hsu P. and Wei J.: Influence of Tibetan Plateau snow cover on East
570   Asian atmospheric circulation at medium-range time scales, Nature communications, 9(1), 4243,
571   2018.
572 Li, Y. and Hu Z.: A Study on Parameterization of Surface Albedo over Grassland Surface in the Northern
573   Tibetan Plateau, Advances in Atmospheric Sciences, 26(1), 161-168, 2009.
574 Liu, H., Hu Z., Yang Y., Wang Y., Sun G. and Huang R.: Simulation of the freezing-thawing processes
575   at Nagqu Area over Qinghai-Xizang Plateau, Plateau Meteorology, 34(003), 676-683, 2015.
576 Liu, X. and Chen B.: Climatic warming in the Tibetan Plateau during recent decades, International
577   Journal of Climatology: A Journal of the Royal Meteorological Society, 20(14), 1729-1742,
578   2000.

Liu, X., Cheng Z., Yan L. and Yin Z.: Elevation dependency of recent and future minimum surface air temperature trends in the Tibetan Plateau and its surroundings, Global and Planetary Change, 68(3), 164–174, 2009.

Ma, W., Ma Y., Li M., Hu Z., Zhong L., Su Z., Ishikawa H. and Wang J.: Estimating surface fluxes over the north Tibetan Plateau area with ASTER imagery, Hydrology and earth system sciences, 13(1), 57-67, 2009.

Ma, Y., Wang Y. and Han C.: Regionalization of land surface heat fluxes over the heterogeneous landscape: from the Tibetan Plateau to the Third Pole region, International Journal of Remote Sensing, 39(18), 5872-5890, 2018.

Ma, Y., Xie Z., Chen Y., Liu S., Che T., Xu Z., Shang L., He X., Meng X., Ma W., Xu B., Zhao H., Wang J., Wu G. and Li X.: Spatially extensive long-term quality-assured land-atmosphere interactions dataset over the Tibetan Plateau, Earth System Science Data Discussions, 2024, 1-37, 2023.

Ma, Y., Yao T., Zhong L., Wang B., Xu X., Hu Z., Ma W., Sun F., Han C., Li M., Chen X., Wang J., Li Y., Gu L., Xie Z., Liu L., Sun G., Wang S., Zhou D., Zuo H., Xu C., Liu X., Wang Y. and Wang Z.: Comprehensive study of energy and water exchange over the Tibetan Plateau: A review and perspective: From GAME/Tibet and CAMP/Tibet to TORP, TPEORP, and TPEITORP, Earth-Science Reviews, 237, 104312, 2023.

Ma, Y., Zhong L., Su Z., Ishikawa H., Menenti M. and Koike T.: Determination of regional distributions and seasonal variations of land surface heat fluxes from Landsat-7 Enhanced Thematic Mapper data over the central Tibetan Plateau area, Journal of Geophysical Research: Atmospheres, 111(D10), 2006.

Qiu, J.: China: the third pole, Nature, 454(7203), 393-397, 2008.

Shen, M., Piao S., Jeong S., Zhou L., Zeng Z., Ciais P., Chen D., Huang M., Jin C., Li L., Li Y., Myneni R., Yang K., Zhang G., Zhang Y. and Yao T.: Evaporative cooling over the Tibetan Plateau induced by vegetation growth, Proceedings of the National Academy of Sciences, 112(30), 9299-9304, 2015.

Shen, Y. and Xiong A.: Validation and comparison of a new gauge-based precipitation analysis over mainland China, International journal of climatology, 36(1), 252-265, 2016.

Song, C., You S., Ke L., Liu G. and Zhong X.: Phenological variation of typical vegetation types in northern Tibet and its response to climate changes, Acta Ecol. Sin, 04, 41–51, 2012.

Su, Y., Zhang Y., Shang L., Wang S., Hu G., Song M., Zhou K.: Root-induced alterations in soil hydrothermal properties in alpine meadows of the Qinghai-Tibet Plateau, Rhizosphere, 20: 100451, 2021.

Sun, C., Xu X., Wang P., Yang D., Zhang S., Wang C. and Cai W.: The warming and wetting ecological environment changes over the Qinghai-Tibetan Plateau and the driving effect of the Asian summer monsoon, Journal of Tropical Meteorology, 28(1), 95-108, 2022.

Sun, G., Hu Z., Ma Y., Xie Z., Wang J. and Yang S.: Simulation Analysis of Local Land Atmosphere Coupling in Rainy Season over a Typical Underlying Surface in the Tibetan Plateau, Hydrology and Earth System Sciences, 24, 5937–5951, 2020.

Sun, G., Hu Z., Ma Y., Xie Z., Yang S. and Wang J.: Analysis of local land-atmosphere coupling in rainy season over a typical underlying surface in Tibetan Plateau based on field measurements and ERA5, Atmospheric Research, 243, 105025, 2020.

Sun, G., Hu Z., Ma Y., Xie Z., Sun F., Wang J. and Yang S.: Analysis of local land atmosphere coupling characteristics over Tibetan Plateau in the dry and rainy seasons using observational data and ERA5, Science of the Total Environment, 774, 145138, 2021.

Sun J., Qin X. and Yang J.: The response of vegetation dynamics of the different alpine grassland types to temperature and precipitation on the Tibetan Plateau, Environmental Monitoring and Assessment, 188(1): 20, 2016.

Sun, J., Yang K., Guo W., Wang Y., He J. and Lu H.: Why has the inner Tibetan Plateau become wetter since the mid-1990s? Journal of Climate, 33(19), 8507-8522, 2020.

Ueno, K., Sugimoto S., Tsutsui H., Taniguchi K., Hu Z. and Wu S.: Role Of Patchy Snow Cover On The Planetary Boundary Layer Structure During Late Winter Observed In The Central Tibetan Plateau, Journal of The Meteorological Society of Japan, 90c, 145-155, 2012.

Wang, G., Hu Z., Yu H., Sun G., Niu R. and Wang X.: Land-atmosphere coupling characteristics in summer based on microwave radiometer data at Nagqu site of Tibetan Plateau, Atmospheric Research, 320, 108074, 2025.

Wang, Y., Liu X., Lv M., Zhang Z.: Mechanisms and influencing factors of hydrothermal processes in active layer soils on the Qinghai-Tibet Plateau under freeze–thaw action, Catena, 220: 106694, 2023.

Wu, G., Liu Y., Zhang Q., Duan A., Wang T., Wan R., Liu X., Li W., Wang Z. and Liang X.: The influence of mechanical and thermal forcing by the Tibetan Plateau on Asian climate, Journal of Hydrometeorology, 8(4), 770-789, 2007.

Wu, G., Liu Y., He B., Bao Q., Duan A. and Jin F.: Thermal Controls on the Asian Summer Monsoon, Scientific reports, 2(1), 404, 2012.

Xie J., Yu Y., Liu C. and Ge J.: Characteristics of Surface Sensible Heat Flux over the Qinghai-Tibetan Plateau and Its Response to Climate Change, Plateau Meteorology, 37(1), 28-42, 2018.

Xie, Z., Ma W., Ma Y., Hu Z., Sun G., Han Y., Hu W., Su R. and Fan Y.: "Decision tree-based detection of blowing snow events in the European Alps, Hydrology and earth system sciences, 25(7), 3783-3804, 2021.

Xie, Z., Ma Y., Ma W., Hu Z. and Sun G.: Comparison of varied complexity parameterizations in estimating blowing snow occurrences, Journal of Hydrology, 619, 129291, 2023.

Yang, K., He J., Tang W., Qin J. and Cheng C.: On downward shortwave and longwave radiations over high altitude regions: Observation and modeling in the Tibetan Plateau, Agricultural and Forest Meteorology, 150(1), 38-46, 2010.

Yang K., Koike T., Fujii H., Tamagawa K. and Hirose N.: Improvement of Surface Flux Parameterizations with a Turbulence-Related Length, Quarterly Journal of Royal Meteorological Society, 128(584), 2073-2087, 2002.

Yang, K., Wu H., Qin J., Lin C., Tang W. and Chen Y.: Recent climate changes over the Tibetan Plateau and their impacts on energy and water cycle: A review, Global and Planetary Change, 112, 79-91, 2014.

Yang, K., Ye B., Zhou D., Wu B., Foken T., Qin J. and Zhou Z.: Response of hydrological cycle to recent climate changes in the Tibetan Plateau, Climatic change, 109, 517-534, 2011.

Yao, T., Thompson L., Yang W., Yu W., Gao Y., Guo X., Yang X., Duan K., Zhao H., Xu B., Pu J., Lu A., Xiang Y., Kattel D. and Joswiak D.: Different glacier status with atmospheric circulations in Tibetan Plateau and surroundings, Nature climate change, 2(9), 663-667, 2012.

665   Zhang, G., Luo W., Chen W. and Zheng G.: A robust but variable lake expansion on the Tibetan Plateau,
666   Science Bull, 64(18), 1306-1309, 2019.

667   Zhang, T., Wang T., Krinner G., Wang X., Gasser T., Peng S., Piao S. and Yao T.: The weakening
668   relationship between Eurasian spring snow cover and Indian summer monsoon rainfall, Science
669   advances, 5(3), eaau8932, 2019.

670   Zhao, Y., Xu X., Liu L., Zhang R., Xu H., Wang Y. and Li J.: Effects of convection over the Tibetan
671   Plateau on rainstorms downstream of the Yangtze River Basin, Atmospheric Research, 219, 24-
672   35, 2019.

673   Zhong, L., Zou M., Ma Y., Huang Z., Xu K., Wang X., Ge N. and Cheng M.: Estimation of downwelling
674   shortwave and longwave radiation in the Tibetan Plateau under all-sky conditions, Journal of
675   Geophysical Research: Atmospheres, 124(21), 11086-11102, 2019.

676   Zou, M., Zhong L., Ma Y., Hu Y. and Feng L.: Estimation of actual evapotranspiration in the Nagqu
677   river basin of the Tibetan Plateau, Theoretical and Applied Climatology, 132(3-4), 1039-1047,
678   2018.

679